Calculation of the inelastic-light-scattering spectrum in ^{4}He in the two-body approximation

J. W. Halley
School of Physics and Astronomy, University of Minnesota, Minneapolis, Minnesota 55455

M. S. Korth and A. J. Wissink
Division of Science and Mathematics, University of Minnesota, Morris, Minnesota 56267
(Received 29 March 1993)

We describe calculations of the inelastic-light-scattering spectrum for frequencies of the order of up to several times the roton frequency. The calculations are based on the two-body approximation in a theoretical description of the fluid due to Manousakis and Pandharipande. On the basis of earlier results we calculate only the contribution arising from quasiparticle anharmonicities in the spectrum and take full account of the strong dependence of the three-quasiparticle coupling on the magnitudes and directions of the momenta of the quasiparticles, which is implied by the two-body approximation. The results are compared with recent experimental results. At high energies, the calculated spectrum is in most respects consistent with the experimental one. We discuss the possible origins of the remaining discrepancies.

I. INTRODUCTION

Though the theoretical literature on the calculation of the second-order inelastic-light-scattering spectrum of superfluid ^{4}He (Refs. 1–3) is extensive,[4–8] we are unaware of an account of a successful first-principles calculation of the observed spectrum. Such a calculation would be significant in establishing a firm understanding of the nature of quasiparticles in ^{4}He and the form of their interactions (which have recently[9] been shown to have an unexpectedly strong momentum dependence).

In the present paper, we present results of a program to make such a first-principles calculation. The goal is not completely achieved for reasons to be discussed below, but the results are in reasonable accord with experiment, and the approach establishes a direction which avoids pitfalls encountered in previous attempts and which can be extended to achieve more exact results. Preliminary results using the same approximations were reported earlier.[9] Some aspects of the results reported here differ from those given in Ref. 9 as a result of corrections in the numerical calculations. In the next section, we discuss the basic formulation of the model and the many-body approach which we are using here. Section III describes calculations of g_3, the three-point coupling constant. In Sec. IV we give results of calculations of the light-scattering spectrum and compare them with experiment. Finally, we present a discussion and conclusions.

II. FUNDAMENTAL THEORETICAL CONSIDERATIONS AND MANY-BODY APPROACH

We start with a rather general expression for the interaction $H_{\rm eff}$ of the electromagnetic field with the fluid:

$$H_{\rm eff}=\int d\mathbf{r}\int d\mathbf{r}'\,\rho(\mathbf{r})\mathbf{E}(\mathbf{r})\cdot\alpha(\mathbf{r},\mathbf{r}')\cdot\mathbf{E}(\mathbf{r}')\rho(\mathbf{r}')\ , \tag{1}$$

where $\rho(\mathbf{r})$ is an operator,

$$\rho(\mathbf{r})=\sum_i \delta(\mathbf{r}-\mathbf{r}_i) \tag{2}$$

($\mathbf{r}_i$ is the position of the ith helium atom), $\mathbf{E}(\mathbf{r})$ is the microscopic electric field, and $\alpha(\mathbf{r},\mathbf{r}')$ is a polarizibility tensor giving the local dipole moment of the medium at the point $\mathbf{r}$, given that there is a field at the point $\mathbf{r}'$. From this coupling one finds that the extinction coefficient $h(\omega)$ is given up to constants, which will not interest us here, by

$$\begin{aligned} h(\omega) &\propto \int \langle H_{\rm eff}(0)H_{\rm eff}(t)\rangle e^{-i\omega t}dt \\ &\propto \int d\mathbf{r}_1\int d\mathbf{r}_2\int d\mathbf{r}_3\int d\mathbf{r}_4\hat{\boldsymbol{\varepsilon}}_0\cdot\alpha(\mathbf{r}_1,\mathbf{r}_2)\cdot\hat{\boldsymbol{\varepsilon}}_n\hat{\boldsymbol{\varepsilon}}_0\cdot\alpha(\mathbf{r}_3,\mathbf{r}_4)\cdot\hat{\boldsymbol{\varepsilon}}_n\langle\rho(\mathbf{r}_1,0)\rho(\mathbf{r}_2,0)\rho(\mathbf{r}_3,t)\rho(\mathbf{r}_4,t)\rangle e^{-i\omega t}dt \\ &\propto \int d^3q\int d^3q' t(\mathbf{q})t(\mathbf{q}')S_2(\mathbf{q},\mathbf{q}',\omega)\ . \end{aligned} \tag{3}$$

Here $\hat{\boldsymbol{\varepsilon}}_0$ and $\hat{\boldsymbol{\varepsilon}}_n$ are, respectively, the polarizations of the incoming and outgoing light in the scattering process. The factors $t(\mathbf{q})$ are defined as

$$t(\mathbf{q})=\int d^3r e^{i\mathbf{q}\cdot\mathbf{r}}\hat{\boldsymbol{\varepsilon}}_0\cdot\alpha(\mathbf{r})\cdot\hat{\boldsymbol{\varepsilon}}_n\ , \tag{4}$$

$$t(\mathbf{q})=t_d(q)\hat{\boldsymbol{\varepsilon}}_0\cdot(3\hat{\mathbf{q}}\hat{\mathbf{q}}-\mathbb{1})\cdot\hat{\boldsymbol{\varepsilon}}_n+t_s(q)\hat{\boldsymbol{\varepsilon}}_0\cdot\hat{\boldsymbol{\varepsilon}}_n\ , \tag{5}$$

0163-1829/93/48(10)/7399(10)/$06.00

in which $t_d(q)=4\pi\int r^2 j_2(qr)\alpha_d(r)dr$ and $t_s(r)=4\pi\int r^2 j_0(qr)\alpha_s(r)dr$. With these developments it then follows that the extinction coefficient can be written in the form

$$h(\omega)\propto I_s(\omega)(\hat{\boldsymbol{\varepsilon}}_0\cdot\hat{\boldsymbol{\varepsilon}}_n)^2+I_d(\omega)[\tfrac{3}{4}+\tfrac{1}{4}(\hat{\boldsymbol{\varepsilon}}_0\cdot\hat{\boldsymbol{\varepsilon}}_n)^2] \ . \tag{6}$$

Here

$$I_d(\omega)=\int 4\pi q^2 dq\int 4\pi q'^2 t_d(q)t_d(q')\tfrac{4}{25}S_2^d(q,q',\omega) \tag{7}$$

and

$$I_s(\omega)=\int 4\pi q^2 dq\int 4\pi q'^2 t_s(q)t_s(q')S_2^s(q,q',\omega) \ . \tag{8}$$

The functions $S_2^{s,d}(q,q',\omega)$ are the $l=0,2$ Legendre projections of the four-point correlation function $S_2(\mathbf{q},\mathbf{q}',\omega)$:

$$S_2^{s,d}(q,q',\omega)=(2l+1)/2\int P_l(\cos\gamma_{\hat{\mathbf{q}},\hat{\mathbf{q}}'})S_2(\mathbf{q},\mathbf{q}',\omega)d\cos\gamma_{\hat{\mathbf{q}},\hat{\mathbf{q}}'} \ , \quad l=0,2 \ . \tag{9}$$

The integrated s-wave scattering is weaker[10] than the d-wave scattering by about a factor of 10 and has been discussed elsewhere.[8] We will not consider it further here.

As we have also discussed elsewhere,[8] the hardest theoretical part of the problem is to be sure that excluded-volume constraints have been correctly included in the calculation of the four-point density-correlation function in these expressions. One approach to a calculation including these effects is described in Refs. 11 and 12. In the language of the present formulation, this work assumes that (up to orthogonalization corrections, which we will not discuss here)

$$\rho_B(\mathbf{k})=\sqrt{Z(\mathbf{k})}(\alpha_{\mathbf{k}}^\dagger+\alpha_{-\mathbf{k}}) \ , \tag{10}$$

where $\alpha_{\mathbf{k}}^\dagger$ and $\alpha_{\mathbf{k}}$ are quasiparticle creation and annihilation operators. The "density" $\rho_B(\mathbf{k})$ is related to the spatial Fourier transform of the particle density through the relation

$$\rho_B(\mathbf{k})=\sum_i^N e^{i\mathbf{k}\cdot\mathbf{r}_i}\left[1+\sum_{j\neq i}\mathbf{k}\cdot\mathbf{r}_{ij}\eta(r_{ij})\right] \ . \tag{11}$$

Without the term involving $\eta(r)$, this would just be the spatial Fourier transform of the particle density. The added term is intended to take account of "backflow" in the variational wave function describing the quasiparticle excitations in a way somewhat like the one used in the original variational calculations of Feynman and Cohen.[13] The function $\eta(r)$ was determined variationally in an approximate way in Ref. 12 where the quasiparticle excited state was assumed to be equal to $\rho_B(\mathbf{k})$ times a Jastrow-like ground state and the energy was minimized with respect to parameters in the function $\eta(r)$. In order to correctly describe the observed quasiparticle spectrum, it was found necessary[11] to assume that these quasiparticles interact according to the quasiparticle Hamiltonian

$$H=\sum_{\mathbf{q}}\varepsilon_{\mathbf{q}}\alpha_{\mathbf{q}}^\dagger\alpha_{\mathbf{q}}+\frac{1}{2}\sum_{\mathbf{q},\mathbf{k}}g_3(\mathbf{q},\mathbf{k})(\alpha_{\mathbf{k}}^\dagger\alpha_{\mathbf{q}}\alpha_{\mathbf{k}-\mathbf{q}}+\alpha_{\mathbf{k}-\mathbf{q}}^\dagger\alpha_{\mathbf{q}}^\dagger\alpha_{\mathbf{k}})$$
$$+\sum_{\mathbf{q},\mathbf{k},\mathbf{l}}g_4(\mathbf{q},\mathbf{k},\mathbf{l})\alpha_{\mathbf{q}}^\dagger\alpha_{\mathbf{k}}^\dagger\alpha_{\mathbf{l}}\alpha_{\mathbf{q}+\mathbf{k}-\mathbf{l}}+\cdots \ . \tag{12}$$

In the approach of Ref. 12, it is possible to calculate the couplings g_3 and g_4 microscopically and they report results for g_3. A full calculation along these lines takes explicit account of the hard core of the helium atoms and should predict the light-scattering spectrum correctly. We report some preliminary results of this sort in the next section. In earlier work[8] we pointed out two possible mechanisms for multiple-quasiparticle structure in the light-scattering spectrum, namely, (1) quasiparticle anharmonicity and (2) nonlinearities in the density-quasiparticle relation. We later showed[9] that only the contribution of the mechanism called "quasiparticle anharmonicity" in Ref. 8 was significant, and we will only consider it here.

We use the two-body approximation of Ref. 11 to calculate the light-scattering spectrum. In principle, one approximates the ground-state function of liquid helium by a wave function of Jastrow variational form:

$$|\Psi_0\rangle=\prod_{1\le i<j\le N}f_J(r_{ij}) \ . \tag{13}$$

In practice, in the two-body approximation, the only properties of the ground state which are needed are those described by the radial distribution function $g(r)$ and its Fourier transform $S(k)$. For this function we follow Refs. 11 and 12 and use experimental values.[14] The variationally calculated $g(r)$ is in reasonably good agreement with experiment, so that the first-principles nature of the calculation is not lost through this use of experimental values. The quasiparticle states are described in a zeroth-order approximation in the scheme of Ref. 11 and 12 by

$$|n\rangle=\rho_B(\mathbf{k}_1)\rho_B(\mathbf{k}_2)\cdots\rho_B(\mathbf{k}_n)|\Psi_0\rangle$$
$$+\text{orthogonalization terms} \ , \tag{14}$$

where $\rho_B(\mathbf{k})$ was defined in (11). The energy of the state $|1\rangle$ is denoted $e_B(\mathbf{k})$. In most of the calculations reported here, we used the "short-range" form of the backflow function discussed in Ref. 11 (but see Sec. III below):

$$\eta(r)=A\exp(-[(r-r_0)/w_0]^2) \ , \tag{15}$$

with the parameters reported by Ref. 11 to minimize the energy of the one-quasiparticle states: $A=0.15$, $r_0=0.8\sigma$, $\omega_0=0.44\sigma$, where $\sigma=2.55$ Å is the hard-core

radius of helium. In the two-body approximation, all the three-body integrals which enter the calculation of matrix elements are dropped. As we will see, this leads to a single-quasiparticle spectrum which is not in extremely good agreement with experiment. Nevertheless, we can learn a great deal about the amplitude of multiparticle signatures in the light-scattering spectrum from such a calculation.

To describe the scattering in terms of this approach, we define the quantity $D_2(\mathbf{q},\mathbf{q}',\omega)$ by

$$D_2(\mathbf{q},\mathbf{q}',\omega)=\langle\Psi_0|\rho(\mathbf{q}')\rho(\mathbf{q}')\left[\frac{1}{H-E_0-\omega-i\varepsilon}\right]\rho(\mathbf{q})\rho(\mathbf{q})|\Psi_0\rangle\ . \tag{16}$$

It is easy to show that

$$2\,\mathrm{Im}D_2(\mathbf{q},\mathbf{q}',\omega)=S_2(\mathbf{q},\mathbf{q}',\omega) \tag{17}$$

as defined above, so that calculation of $D(\mathbf{q},\mathbf{q},\omega)$ will give us the needed function. As in Ref. 12, we let $H=H_0+H_I$, where H_0 is diagonal in the states (14), and make a perturbation expansion in H_I. If we expand the operators $\rho(\mathbf{q})$ in terms of the operators $\rho_B(\mathbf{q})$ using (11) and take the first term, we get a description in terms of a two-quasiparticle bare propagator and its interactions. (A discussion of the contribution of the next term in the expansion of ρ_B in terms of ρ appears in Ref. 9.) We select a subset of the perturbation series corresponding to ignoring the interaction between the quasiparticles but including all their self-energy corrections. Then we obtain

$$D_2(\mathbf{q},\mathbf{q}',\omega)=-\langle\Psi_0|\rho_B(\mathbf{q})\rho_B(-\mathbf{q})|\mathbf{q},-\mathbf{q}\rangle|^2\delta_{\mathbf{q},-\mathbf{q}'}\times\int\frac{d\omega'}{2\pi i}\frac{1}{e_B(\mathbf{q})+\Sigma(\mathbf{q},\omega-\omega')-(\omega-\omega')-i\varepsilon}\frac{1}{e_B(-\mathbf{q})+\Sigma(-\mathbf{q},\omega')-\omega'-i\varepsilon}\ , \tag{18}$$

where Σ is the self-energy. The state $|\mathbf{q},-\mathbf{q}\rangle$ is the normalized and orthogonalized two-quasiparticle state defined by (14). In the calculations reported here, we have approximated the matrix element whose square appears in front of the integral as $\langle\Psi_0|\rho_B(\mathbf{q})|\mathbf{q}\rangle|\mathbf{q}\rangle\equiv N_{\mathbf{q},\mathbf{q}}$. It is important to note that this approximation can contribute to violations of the hard-core constraint discussed in the Introduction, and we hope to improve on it. The integration in (18) is done by use of Cauchy's theorem. We define the complex numbers z_i', $i=1\ldots,n$, as the solutions to the equation

$$z_i'=e_B(-\mathbf{q})+\Sigma(-\mathbf{q},z_i')-i\varepsilon\ , \tag{19}$$

giving

$$D_2(\mathbf{q},\mathbf{q}',\omega)=\sum_{i=1}^{n}\frac{|\langle\Psi_0|\rho_B(\mathbf{q})|\mathbf{q}\rangle|^2\delta_{\mathbf{q},-\mathbf{q}'}}{e_B(\mathbf{q})+e_B(-\mathbf{q})+\Sigma(-\mathbf{q},z_i')+\Sigma(\mathbf{q},\omega-z_i')-\omega-2i\varepsilon}\ . \tag{20}$$

It is quite feasible to evaluate the spectrum using this expression. However, for numerical simplicity we make the additional assumptions that (1) we can replace z_i' in the arguments of the self-energies of the last equation by its real part and (2) the contribution of the pole i to the sum in the last expression is dominantly near

$\omega=e_{\mathrm{sc}}^i(\mathbf{q})+e_{\mathrm{sc}}^i(-\mathbf{q})$, where $e_{\mathrm{sc}}^i(\mathbf{q})$ is a solution to

$$e_{\mathrm{sc}}^i(\mathbf{q})=e_B(\mathbf{q})+\mathrm{Re}\Sigma(\mathbf{q},e_{\mathrm{sc}}^i(\mathbf{q}))\ . \tag{21}$$

With these further assumptions, the expression for $D_2(\mathbf{q},\mathbf{q},\omega)$ becomes

$$\sum_{i=1}^{n}\frac{|N_{\mathbf{q},\mathbf{q}}|^2}{2e_{\mathrm{sc}}^i(\mathbf{q})+2i\,\mathrm{Im}\Sigma(\mathbf{q},e_{\mathrm{sc}}^i(\mathbf{q}))-\omega-2i\varepsilon}\ . \tag{22}$$

This has an obvious physical interpretation. To evaluate it we need to compute the self-energy function arising from the perturbation expansion.

To evaluate the self-energy, we use the lowest-order expression

$$\mathrm{Im}\Sigma(\mathbf{k},\omega)=-\frac{\pi}{2}\sum_{\mathbf{l},\mathbf{m}}|g_3(\mathbf{k},\mathbf{l})|^2\delta[\omega-e_B(\mathbf{l})-e_B(\mathbf{m})]\ . \tag{23}$$

[A better approximation would be to use the solutions to Eq. (21) in place of e_B in the self-energy and solve the last equation and Eq. (21) together.] To evaluate the real part of the self-energy, we use the Kramers-Kronig relation, as in Ref. 12. At large momenta it is not hard to show that, because all the bare spectra become free particle like, the real part of the self-energy acquires a divergence, so that it increases with the square root of the upper limit of the Kramers-Kronig integral. We made a preliminary exploration of the effects of this on our calculations by studying the self-energy as a function of momentum cutoff and of frequency at high frequencies. We conclude that the divergence does not strongly affect our results, but its existence is a reason for treating the application of these approximations with caution.

To evaluate this form of the self-energy, we need expressions for the bare quasiparticle spectrum $e_B(\mathbf{k})$ and

the three-quasiparticle coupling $g_3(\mathbf{k},\mathbf{l})$, which can be evaluated in terms of the experimental $g(r)$ and the variational function $\eta(r)$. Following Refs. 11 and 12, we evaluated $e_B(\mathbf{k})$ from the expression

$$e_B(k)=H_{11}(k)/N_{11}(k) , \tag{24}$$

in which

$$H_{11}=\frac{\hbar^2}{2m}\sum_i \langle \Psi_0|\nabla_i\rho_B^\dagger(\mathbf{k})\cdot\nabla_i\rho_B(\mathbf{k})|\Psi_0\rangle , \tag{25}$$

$$N_{11}=\langle \Psi_0|\rho_B^\dagger(\mathbf{k})\rho_B(\mathbf{k})|\Psi_0\rangle . \tag{26}$$

The integrals needed for evaluation of H_{11} and N_{11} are summarized in Appendix A. The evaluation of $g_3(\mathbf{k},\mathbf{l})$, which resulted in the most unexpected results reported here, is described in the next section.

To finally evaluate the light-scattering spectrum, we need expressions for the function $t_d(q)$, which describes the coupling of the light to the fluid. We made a fit to the anisotropic part of the pair polarizibility of helium as reported by Dacre,[15] which takes the analytical form

$$\alpha_d(r)=\frac{A}{(Br^3+C)}(1-e^{-Dr^3}) , \tag{27}$$

in which $A=11.4264$ Å^3, $B=6.748$ Å^{-3}, $C=2.0$, and $D=0.108$ Å^{-3}. The effects of using other forms[16] for $t_d(q)$ are discussed in Ref. 9.

III. EVALUATION OF g_3

The three-quasiparticle coupling $g_3(\mathbf{k},\mathbf{l})$ appearing in (23) is defined by the expression

$$g_3(\mathbf{k},\mathbf{l})=\langle \mathbf{l},\mathbf{k}-\mathbf{l}|H-E_0|\mathbf{k}\rangle , \tag{28}$$

where $|\mathbf{k}\rangle$ and $|\mathbf{l},\mathbf{k}-\mathbf{l}\rangle$ are orthonormalized one- and two-quasiparticle states, respectively. We will let $\mathbf{m}=\mathbf{k}-\mathbf{l}$ in what follows. Before orthonormalization, the quasiparticle states are described by

$$|\Psi_{\mathbf{k}}\rangle=\rho_B(\mathbf{k})|\Psi_0\rangle \tag{29}$$

and

$$|\Psi_{\mathbf{l},\mathbf{k}-\mathbf{l}}\rangle=\rho_B(\mathbf{l})\rho_B(\mathbf{k}-\mathbf{l})|\Psi_0\rangle . \tag{30}$$

Then

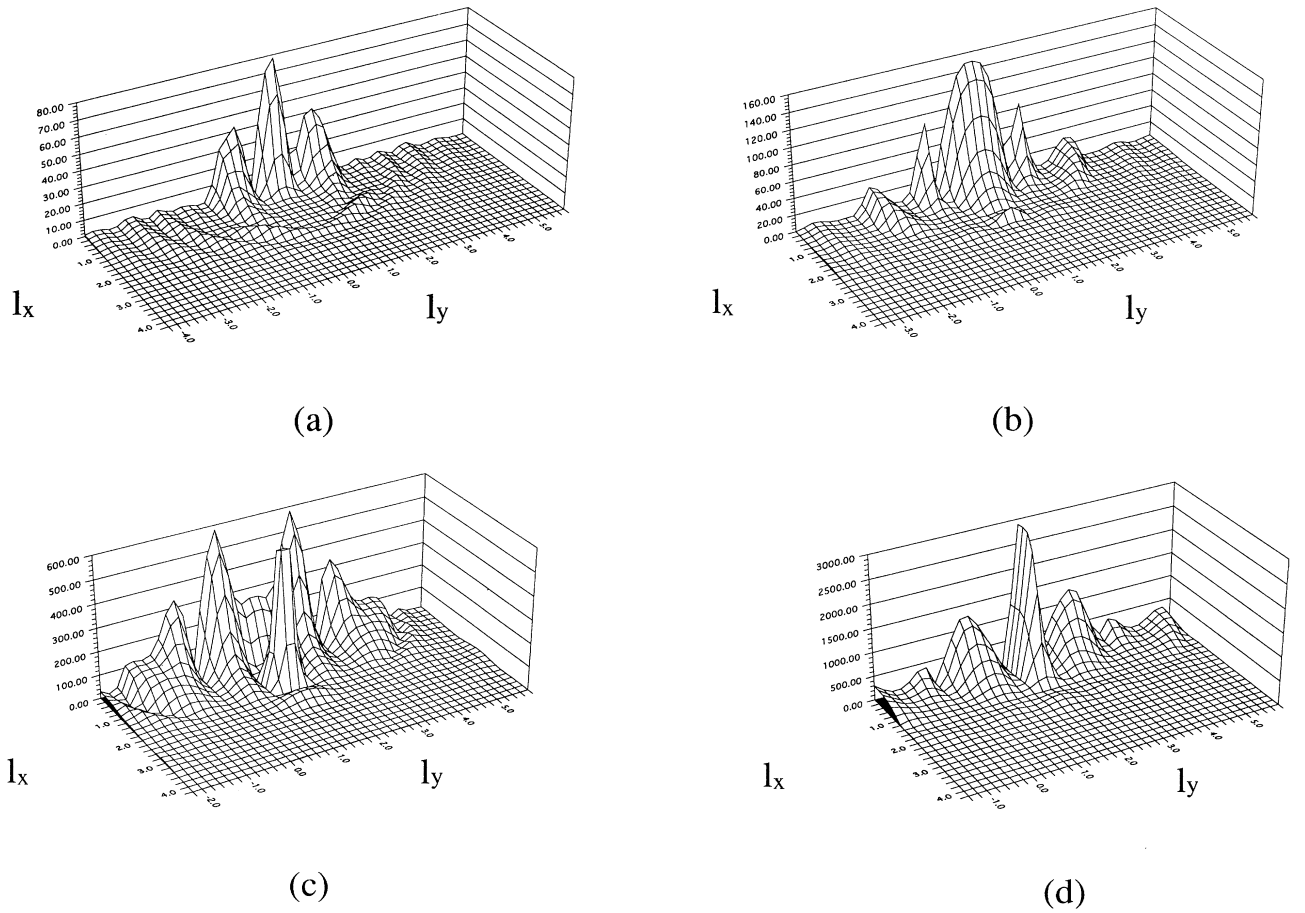

FIG. 1. Coupling functions $|g_3(\mathbf{k},\mathbf{l})|^2$ for various values of $|\mathbf{k}|$. $\mathbf{k}$ lies along the x axis, and the two axes denote the x and y components of $\mathbf{l}$. (a) $|\mathbf{k}|=1.08$ Å^{-1}, (b) $|\mathbf{k}|=1.92$ Å^{-1}, (c) $|\mathbf{k}|=3.00$ Å^{-1}, and (d) $|\mathbf{k}|=3.96$ Å^{-1}.

$$g_3(\mathbf{k},\mathbf{l})=\frac{H_{21}N_{11}-H_{11}N_{12}}{N_{11}\sqrt{N_{11}N_{22}}} . \tag{31}$$

H_{11} and N_{11} also appear in the expression for the bare quasiparticle energy $e_B(k)$ [Eq. (24)] and are defined in Eqs. (25) and (26). The integrals required for their evaluation are summarized in Appendix A. H_{12}, N_{12}, and N_{22} are defined as

$$H_{21}=\frac{\hbar^2}{2m}\sum_i \langle\Psi_0|\nabla_i[\rho_B^\dagger(\mathbf{l})\rho_B^\dagger(\mathbf{k}-\mathbf{l})]\cdot\nabla_i\rho_B(\mathbf{k})|\Psi_0\rangle , \tag{32}$$

$$N_{12}=\langle\Psi_0|\rho_B^\dagger(\mathbf{l})\rho_B^\dagger(\mathbf{k}-\mathbf{l})\rho_B(\mathbf{k})|\Psi_0\rangle , \tag{33}$$

and

$$N_{22}=N_{11}N_{11} . \tag{34}$$

Integrals required for the evaluation of H_{12} and N_{12} are summarized in Appendixes B and C, respectively.

The integrals were evaluated using standard numerical techniques. Many of the integrals are rapidly oscillating functions because of the presence of the complex exponential. These were evaluated using a fast-Fourier-transform algorithm, which was checked against the appropriate IMSL routine. The remaining integrations were performed using a trapezoidal rule on a grid that is successively halved until an acceptable convergence is reached. This process is equivalent to Simpson's rule.[17] We show values of $g_3(\mathbf{k},\mathbf{l})$ for a few values of $\mathbf{k}$ in Fig. 1.

In order to ascertain whether the structures found in $g_3(\mathbf{k},\mathbf{l})$ are due to the particular form of the backflow function $\eta(r)$ used as well as the sensitivity of the calculation to that function, we repeated the calculations using two other functions. The first of these was a (monotonic) power-law form

$$\eta_2(r)=\frac{A}{r^6} , \tag{35}$$

where $A=40$ Å^6. We also tried an $\eta_3(r)$ which is functionally identical to Eq. (15) but with slightly altered parameters ($A=0.096$, $r_0=0.8\sigma$, $w_0=0.62\sigma$) which yield

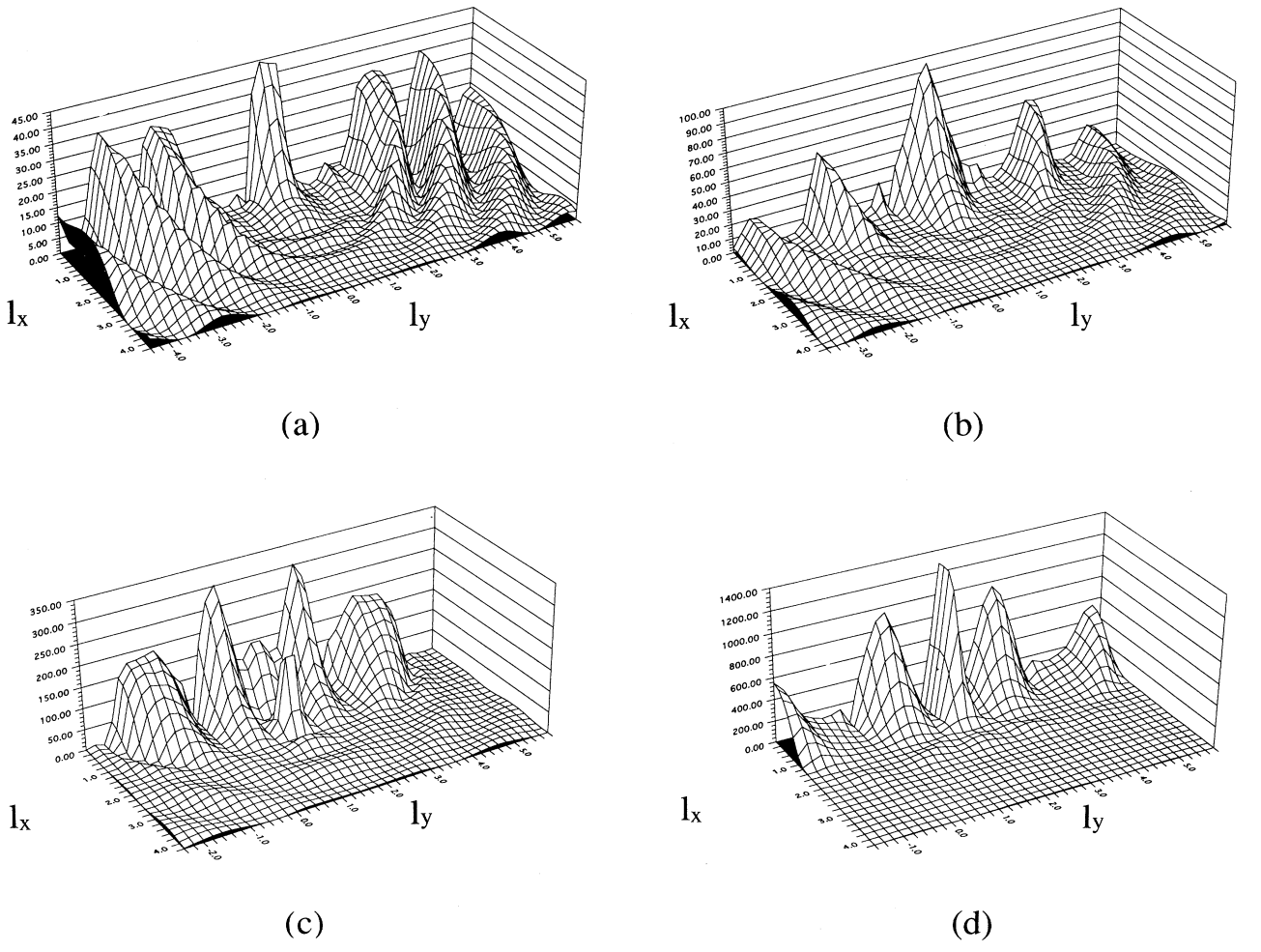

FIG. 2. Same as Fig. 1, but with g_3 calculated using the backflow function η_2.

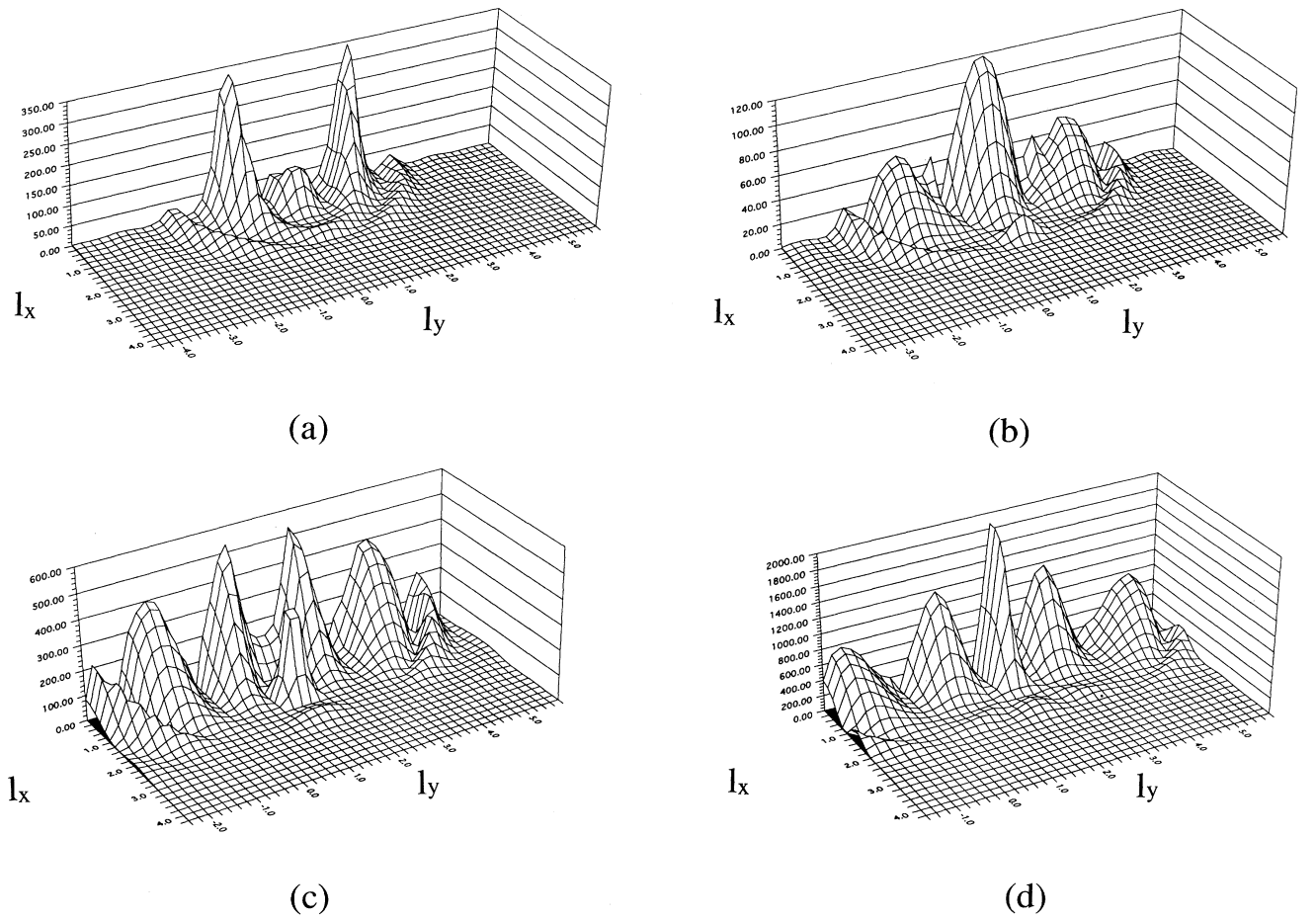

FIG. 3. Same as Fig. 1, but with g_3 calculated using the backflow function η_3.

a backflow function less sharply peaked than the variationally optimized one. Both alternative backflow functions result in values of $g_3(\mathbf{k},\mathbf{l})$ qualitatively similar to those obtained with the earlier $\eta(r)$ as shown in Figs. 2 and 3, which should be compared with Fig. 1. Quantitatively, the heights and locations of peaks vary between the three cases in a fashion that is not simple to characterize. Nevertheless, we note that, with respect to variations in the backflow function, g_3 remains a complicated function of momenta in which collinear processes are favored.

IV. RESULTS FOR THE LIGHT-SCATTERING SPECTRUM

We show solutions to the Eq. (21) in Fig. 4. [Some details concerning the method of solution of (21) appear in the next paragraph.] There is a very sharp quasiparticle branch and many broader multiparticle branches. The quasiparticle spectrum differs from the experimental one[18] by as much as 20%. In particular, the maxon energy is 12.5 K compared to the experimental value of 13.8 K and the roton energy is 10.8 K compared to the experimental value of 8.7 K. As a result of this, peaks in a calculated light-scattering spectrum would not appear at the proper energies.

The correct way to improve the quasiparticle spectrum is to go to a better approximation, such as the extended two-body approximation of Ref. 12. However, as dis-

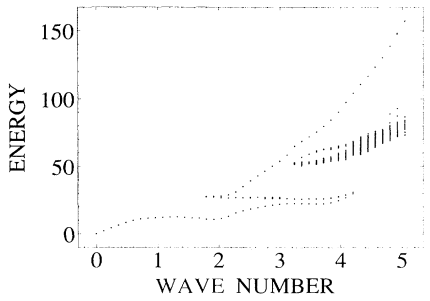

FIG. 4. Self-consistent energy spectrum e^1_{sc} from Eq. (21) using the bare spectrum from the two-body approximation of Refs. 11 and 12.

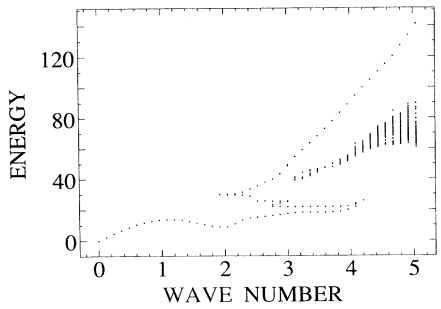

FIG. 5. Same as Fig. 4, but with the empirical bare spectrum $e'_B(k)$ used to calculate $e'_{sc}(k)$ from (21).

cussed in Ref. 9, we have done the calculation of the spectrum again using an empirical bare spectrum $e'_B(\mathbf{q})$, which is chosen to give a quasiparticle spectrum $e^1_{sc}(\mathbf{q})$ which agrees with experiment. The results of solving (21) using the empirical bare spectrum are compared with the experimental quasiparticle spectrum in Fig. 5. Figure 6 displays some graphical features of the solution to (21) using $e'_B(\mathbf{q})$.

The light-scattering spectrum calculated using $e'_B(\mathbf{q})$ in Eqs. (21)–(23) is shown in Fig. 7. The peaks correspond to frequencies such as those which would be identified as multiparticle peaks in the experimental spectrum. By making a series of partial calculations, we are able to identify all of the structures appearing in this calculated spectrum as discussed in the next section.

In Fig. 8 we show the results of convoluting our calculated spectrum with a Gaussian with energy width corresponding to the reported energy resolution in Ref. 19. The experimental data[19] are also shown in Fig. 8. (The experimental intensities were all multiplied by an arbitrary scale factor in order to approximately match the calculated ones.) Many of the same features are observed, though detailed shapes are different and the calculated spectrum is consistently shifted to somewhat higher energies by a few degrees kelvin relative to the observed one.

V. DISCUSSION

The structure revealed in the graphs of $g_3(\mathbf{k},\mathbf{l})$ in Fig. 1 is quite interesting and partly unexpected. When $|\mathbf{k}|$ corresponds to a maxon (≈ 1 Å^{-1}) as in Fig. 1(a), we find three large peaks in $g_3(\mathbf{k},\mathbf{l})$ which correspond to interactions in which $\mathbf{k}$ and $\mathbf{m}=\mathbf{k}-\mathbf{l}$ are all approximately collinear. Two of the peaks correspond to processes of decay of the maxon into one roton plus one maxon. The other (central) peak corresponds to a process of decay into two phonons. The latter is not anticipated on simple intuitive grounds. When $|\mathbf{k}|$ corresponds to a roton (≈ 1.9 Å^{-1}) as in Fig. 1(b), we find five peaks associated with collinear processes. The largest (central) peak corresponds to decay into a pair of maxons. The pair of next largest peaks is associated with decay of the roton into one phonon plus one excitation near 2.2 Å^{-1}. The remaining pair of peaks corresponds to decay into a 1.5-Å^{-1} quasiparticle plus a quasiparticle associated with the plateau which occurs near 3.4 Å^{-1} in our calculated energy spectrum. (See below.) It is important to also note a small off-axis peak near $\mathbf{l}=(1.0\ \text{Å}^{-1})\hat{\mathbf{x}}+(1.8\ \text{Å}^{-1})\hat{\mathbf{y}}$ which corresponds to decay into two rotons. At larger values of $|\mathbf{k}|$, the peak corresponding to decay into two

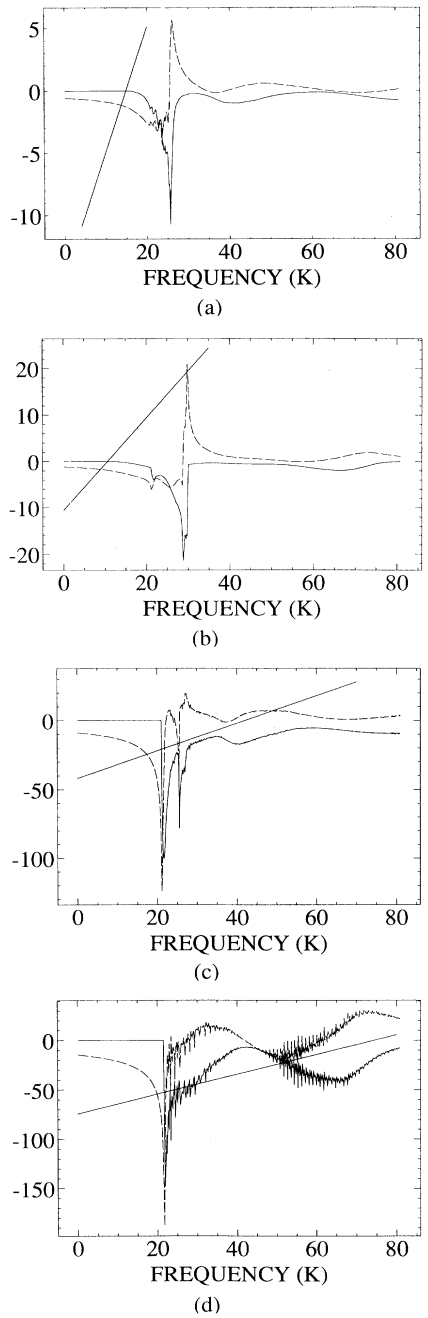

FIG. 6. Graphical representation of the solutions of Eq. (21) for various values of $|\mathbf{k}|$ using the empirical bare spectrum. The real (dashed curve)and imaginary (solid curve) parts of the self-energy are shown together with the (solid) straight line $\omega-e(k)$. (a) $|\mathbf{k}|=1.08$ Å^{-1}, (b) $|\mathbf{k}|=1.92$ Å^{-1}, (c) $|\mathbf{k}|=3.00$ Å^{-1}, and (d) $|\mathbf{k}|=3.96$ Å^{-1}.

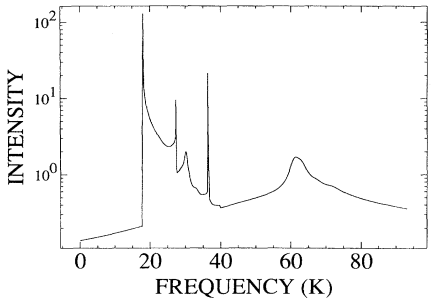

FIG. 7. Calculated light-scattering spectrum.

rotons gains in strength and moves toward the x axis. (The latter occurs because **k**, **l**, and **m** must form a closed triangle, in this case an isosceles triangle.) It should be kept in mind that $g_3(\mathbf{k},\mathbf{l})$ for a given **k** is a function of three dimensions and is obtained by rotating the graphs shown about the x axis. Thus off-axis peaks are more important, relative to on-axis peaks, than they might appear. Figures 1(c) and 1(d) help to illustrate that $g_3(\mathbf{k},\mathbf{l})$ continues to be a complicated function of the magnitude and direction of **l** and that collinear processes continue to be important at all $|\mathbf{k}|$ values.

The empirical spectrum leads to a lowest single-quasiparticle branch (Fig. 5) which is quite similar to experimental results[18] for all wave vectors. (The previously reported drop[9] in this branch at 3.4 Å^{-1} was due to a numerical artifact.) The relative flatness of the spectrum from 2.5 to 4 Å^{-1} is a result of the strong coupling g_3 for decay into two rotons. (This results in the off-axis peak in g_3 discussed above.) At higher energies the predicted multiphonon energies are qualitatively consistent with the neutron results except that the calculated multiphonon spectrum begins at a higher wave vector (about 2 Å^{-1}) than the experimental one. Within our approximations the neutron-scattering function will have multiparticle weight below this momentum because of the imaginary part of the self-energy.

The calculated light-scattering spectrum is broadly similar to the experimental one except for the predicted peak at 60 K. This peak arises from a double excitation of the onset in the calculated self-consistent multiphonon particle spectrum at 2 Å^{-1} as seen in Fig. 5. As just discussed, this feature of the multiparticle spectrum is not observed in neutron-scattering experiments and is probably a defect of the two-body approximation. It does not appear in the results of Ref. 12. The peak at 27.2 K corresponds to two maxons, the peak at 30.0 K to two excitations of wave number near 2.4 Å^{-1}, and the peak at 36.4 K can be unambiguously identified with two excitations of wave number near 3.6 Å^{-1}. The last of these can be thought of as a four-roton effect since the flatness of the energy spectrum near 3.6 Å^{-1} is due to the strong coupling of this excitation to two rotons.

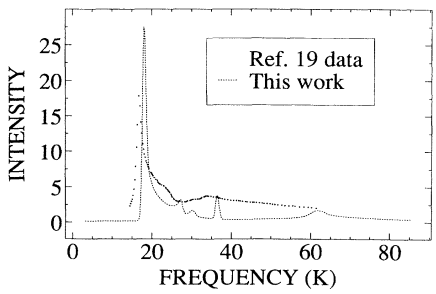

FIG. 8. Light-scattering spectrum convoluted with a Gaussian of a full width at half maximum (FWHM) $=1.0$ K compared with the experimental data of Ref. 19.

VI. CONCLUSIONS

We have described a calculation of the light-scattering spectrum in the two-body approximation of Refs. 11 and 12. Some details of the treatment of the calculation of the two-quasiparticle propagator differ from that of those authors. The coupling functions $g_3(\mathbf{k},\mathbf{l})$ are very strong functions of the magnitudes and directions of their vector arguments. In particular, processes in which the wave vectors are parallel are strongly favored. We showed that these general features of g_3 persist when other forms of the backflow function η are used in the definition of the quasiparticle wave-function basis. In the calculated function g_3, processes in which the wave vectors are all parallel are strongly favored. We calculated the light-scattering spectrum arising from these coupling functions, using an empirical bare quasiparticle spectrum which reproduces the experimental spectrum self-consistently at low momenta.

In calculating the light-scattering spectrum, we used a matrix element $t_d(q)$ consistent with current understanding of the pair polarizibility of helium. The resulting spectrum looks qualitatively like the experimental one except for a feature at 60 K, which is likely to be an artifact of our approximations. The fact that the experimental spectrum has most features somewhat lower in energy than the calculated spectrum is probably a consequence of the omission of four-point quasiparticle interactions (g_4) in our dynamic calculation. The two-body approximation can be used to calculate g_4, and the resulting Bethe-Salpeter equation for the interacting two quasiparticle propagator could be solved. At this level a shift somewhat like the experimentally observed one can be anticipated.

To further improve the approximations made here, one can contemplate either implementation of the extended two-body approximation of Refs. 11 and 12 or Monte Carlo evaluation of the relevant integrals for evaluation of the quasiparticle parameters ε_B and g_3,g_4. The latter approach is more feasible than the former as a result of improved computational capabilities.

ACKNOWLEDGMENTS

We wish to thank the Minnesota Supercomputer Institute, the University of Minnesota Graduate School, the Research Corporation, and the University of Minnesota at Morris for support.

APPENDIX A: DEFINITIONS OF MATRIX ELEMENTS NEEDED IN THE CALCULATION OF $e_B(k)$

The matrix elements $N_{11}(k)$ and $H_{12}(k)$ which are required [see (24)] are written as

$$N_{11}(k)=[1+I_9/2]^2S(k)+\bar{I}_{10} , \tag{A1}$$

$$H_{11}(k)=\frac{\hbar^2k^2}{2m}[1+I_1+I_2+k^2I_3+I_{457}+kI_6] . \tag{A2}$$

The integrals I_i which appear in these expressions are in turn expressed in terms of calculable integrals as

$$I_1=2\rho\int d^3r\, g(r)\hat{\mathbf{k}}\cdot\nabla[\eta(r)\hat{\mathbf{k}}\cdot\mathbf{r}] , \tag{A3}$$

$$I_2(k)=-2\rho\int d^3r\, g(r)e^{i\mathbf{k}\cdot\mathbf{r}}\hat{\mathbf{k}}\cdot\nabla[\eta(r)\hat{\mathbf{k}}\cdot\mathbf{r}] , \tag{A4}$$

$$I_3=\frac{\rho}{3}\int d^3r\, r^2g(r)\eta(r)\eta(r) , \tag{A5}$$

$$I_3^{\rm ex}(k)=-\rho\int d^3r\, g(r)e^{i\mathbf{k}\cdot\mathbf{r}}\eta(r)^2(\hat{\mathbf{k}}\cdot\mathbf{r})^2 , \tag{A6}$$

$$I_{457}(k)=\tfrac{1}{4}[I_1+I_2]^2+\rho\int d^3r g(r)(\nabla[\eta(r)\hat{\mathbf{k}}\cdot\mathbf{r}])^2\times(2-e^{i\mathbf{k}\cdot\mathbf{r}}-e^{-i\mathbf{k}\cdot\mathbf{r}}) , \tag{A7}$$

$$I_6(k)=-\rho\int d^3r\, g(r)\eta(r)(\hat{\mathbf{k}}\cdot\mathbf{r})\hat{\mathbf{k}}\cdot\nabla[\eta(r)\hat{\mathbf{k}}\cdot\mathbf{r}]\times i(e^{i\mathbf{k}\cdot\mathbf{r}}-e^{-i\mathbf{k}\cdot\mathbf{r}}) , \tag{A8}$$

$$I_9(k)=2i\rho\int d^3r\, g(r)\eta(r)(\mathbf{k}\cdot\mathbf{r})e^{i\mathbf{k}\cdot\mathbf{r}} , \tag{A9}$$

$$I_{10}(k)=S(k)[I_9(k)]^2+\bar{I}_{10}(k) , \tag{A10}$$

$$\bar{I}_{10}(k)=k^2[I_3+I_3^{\rm ex}(k)] . \tag{A11}$$

APPENDIX B: INTEGRALS REQUIRED FOR THE EVALUATION OF H_{12}

Using the definition (32), one finds

$$H_{21}(\mathbf{k},\mathbf{l},\mathbf{m})=T_1(\mathbf{k},\mathbf{l},\mathbf{m})+T_2(\mathbf{k},\mathbf{l},\mathbf{m})+T_3(\mathbf{k},\mathbf{l},\mathbf{m})+T_1(\mathbf{k},\mathbf{m},\mathbf{l})+T_2(\mathbf{k},\mathbf{m},\mathbf{l})+T_3(\mathbf{k},\mathbf{m},\mathbf{l}) . \tag{B1}$$

The integrals T_i are defined as

$$T_1(\mathbf{k},\mathbf{l},\mathbf{m})=\mathbf{k}\cdot\mathbf{l}\left[\frac{2m}{\hbar^2k^2}H_{11}(k)-\mathbf{k}\cdot\mathbf{m}I_3\right][S_B(m)-1] , \tag{B2}$$

$$T_2(\mathbf{k},\mathbf{l},\mathbf{m})=[Q(l)U_1(\mathbf{k},\mathbf{l},\mathbf{m})+Q(k)U_2(\mathbf{k},\mathbf{l},\mathbf{m})+U_3(\mathbf{k},\mathbf{l},\mathbf{m})]S_B(m) , \tag{B3}$$

$$T_3(\mathbf{k},\mathbf{l},\mathbf{m})=[Q(k)W_1(\mathbf{k},\mathbf{l},\mathbf{m})+Q(l)W_2(\mathbf{k},\mathbf{l},\mathbf{m})+W_3(\mathbf{k},\mathbf{l},\mathbf{m})] , \tag{B4}$$

T_1 involves only H_{11}, I_3 (see Appendix A), and S_B (defined in Appendix C). T_2 involves Q, defined as

$$Q(k)=1+\tfrac{1}{2}[I_1+I_2(k)] . \tag{B5}$$

I_1 and I_2 are defined in Appendix A.

T_2 also involves the quantities U_1, U_2, and U_3, which are defined in terms of calculable integrals as

$$U_1(\mathbf{k},\mathbf{l},\mathbf{m})=i\rho\mathbf{k}\cdot\mathbf{l}\int d^3r\, g(r)\eta(r)(\mathbf{k}\cdot\mathbf{r})e^{i\mathbf{m}\cdot\mathbf{r}}+\rho\int d^3r\, g(r)\nabla[\eta(r)\mathbf{k}\cdot\mathbf{r}]\cdot\mathbf{l}(e^{i\mathbf{m}\cdot\mathbf{r}}-e^{i\mathbf{l}\cdot\mathbf{r}}) , \tag{B6}$$

$$U_2(\mathbf{k},\mathbf{l},\mathbf{m})=-i\rho\mathbf{k}\cdot\mathbf{l}\int d^3r\, g(r)\eta(r)(\mathbf{l}\cdot\mathbf{r})e^{i\mathbf{m}\cdot\mathbf{r}}\rho\int d^3r\, g(r)\nabla[\eta(r)\mathbf{l}\cdot\mathbf{r}]\cdot\mathbf{k}(e^{i\mathbf{m}\cdot\mathbf{r}}-e^{i\mathbf{l}\cdot\mathbf{r}}) , \tag{B7}$$

$$\begin{aligned}U_3(\mathbf{k},\mathbf{l},\mathbf{m})=&\rho(\mathbf{k}\cdot\mathbf{l})\int d^3r\, g(r)\eta(r)^2(\mathbf{k}\cdot\mathbf{r})(\mathbf{l}\cdot\mathbf{r})e^{i\mathbf{m}\cdot\mathbf{r}}\\&+\rho\int d^3r\, g(r)(-i\eta(r)(\mathbf{l}\cdot\mathbf{r})\{\mathbf{l}\cdot\nabla[\eta(r)(\mathbf{k}\cdot\mathbf{r})]\}+i(\mathbf{k}\cdot\mathbf{r})\eta(r)\{\mathbf{k}\cdot\nabla[\eta(r)(\mathbf{l}\cdot\mathbf{r})]\}\\&\quad+2\nabla[\eta(r)(\mathbf{k}\cdot\mathbf{r})]\cdot\nabla[\eta(r)(\mathbf{l}\cdot\mathbf{r})])e^{i\mathbf{m}\cdot\mathbf{r}}\\&-\rho\int d^3r\, g(r)(i\eta(r)(\mathbf{l}\cdot\mathbf{r})\{\mathbf{l}\cdot\nabla[\eta(r)(\mathbf{k}\cdot\mathbf{r})]\}+i(\mathbf{k}\cdot\mathbf{r})\eta(r)\{\mathbf{k}\cdot\nabla[\eta(r)(\mathbf{l}\cdot\mathbf{r})]\}\\&\quad+2\nabla[\eta(r)(\mathbf{k}\cdot\mathbf{r})]\cdot\nabla[\eta(r)(\mathbf{l}\cdot\mathbf{r})])e^{i\mathbf{l}\cdot\mathbf{r}} .\end{aligned} \tag{B8}$$

Finally, T_3 involves Q, S_B, and the terms W_1, W_2, and W_3, which are defined as

$$W_1(\mathbf{k},\mathbf{l},\mathbf{m})=\rho(\mathbf{k}\cdot\mathbf{l})\int d^3r\, g(r)\eta(r)^2(\mathbf{l}\cdot\mathbf{r})(\mathbf{m}\cdot\mathbf{r})e^{i\mathbf{m}\cdot\mathbf{r}}+i\rho\int d^3r\, g(r)\eta(r)(\mathbf{m}\cdot\mathbf{r})\{\mathbf{k}\cdot\nabla[\eta(r)(\mathbf{l}\cdot\mathbf{r})]\}(e^{i\mathbf{m}\cdot\mathbf{r}}+e^{i\mathbf{l}\cdot\mathbf{r}}) , \tag{B9}$$

$$W_2(\mathbf{k},\mathbf{l},\mathbf{m})=-\rho(\mathbf{k}\cdot\mathbf{l})\int d^3r\, g(r)\eta(r)^2(\mathbf{k}\cdot\mathbf{r})(\mathbf{m}\cdot\mathbf{r})e^{i\mathbf{m}\cdot\mathbf{r}}+i\rho\int d^3r\, g(r)\eta(r)(\mathbf{m}\cdot\mathbf{r})\{\mathbf{l}\cdot\nabla[\eta(r)(\mathbf{k}\cdot\mathbf{r})]\}(e^{i\mathbf{m}\cdot\mathbf{r}}+e^{i\mathbf{l}\cdot\mathbf{r}}) , \tag{B10}$$

$$W_3(\mathbf{k},\mathbf{l},\mathbf{m})=-\rho^2\int d^3r\, g(r)e^{i\mathbf{l}\cdot\mathbf{r}}\nabla[\eta(r)\mathbf{l}\cdot\mathbf{r}]\left[-i\int d^3r'\, g(r')\eta(r')\mathbf{m}\cdot\mathbf{r}'\nabla'[\eta(r')\mathbf{k}\cdot\mathbf{r}']e^{i\mathbf{k}\cdot\mathbf{r}'}+\mathbf{k}\int d^3r'\, g(r')\eta^2(r')(\mathbf{m}\cdot\mathbf{r}')(\mathbf{k}\cdot\mathbf{r}')\right] . \tag{B11}$$

APPENDIX C: INTEGRALS REQUIRED FOR THE EVALUATION OF N_{21}

Using the definition (26), one finds the expression

$$N_{21}(\mathbf{k},\mathbf{l},\mathbf{m})=\sigma_1+\sigma_{2i}+\sigma_{2j}+\sigma_{2n}+\sigma_{3ij}+\sigma_{3jn}+\sigma_{3in} \ . \tag{C1}$$

The integrals $\sigma,\ldots$ are defined in terms of the quantity

$$S_B(k)=S(k)[1+\tfrac{1}{2}I_9(k)] \ , \tag{C2}$$

in which $S(k)$ is the experimental structure function and I_9 is defined in Appendix A. In terms of $S_B(k)$, the quantities $\sigma,\ldots$ are expressed as

$$\sigma_1=S_B(k)[S_B(l)S_B(m)-1] \ , \tag{C3}$$

$$\sigma_{2i}=\frac{1}{2}\left[\frac{\mathbf{k}\cdot\mathbf{m}}{m^2}I_9(m)+\frac{\mathbf{k}\cdot\mathbf{l}}{l^2}I_9(l)\right]S_B(l)S_B(m) \ , \tag{C4}$$

$$\sigma_{2j}=\frac{1}{2}\left[\frac{\mathbf{k}\cdot\mathbf{l}}{k^2}I_9(k)\left[S_B(m)-1\right]-\frac{\mathbf{l}\cdot\mathbf{m}}{m^2}I_9(m)S_B(m)\right]S_B(k) \ , \tag{C5}$$

$$\sigma_{2n}=\frac{1}{2}\left[\frac{\mathbf{k}\cdot\mathbf{m}}{k^2}I_9(k)\left[S_B(l)-1\right]-\frac{\mathbf{m}\cdot\mathbf{l}}{l^2}I_9(l)S_B(l)\right]S_B(k) \ , \tag{C6}$$

$$\sigma_{3jn}=\rho S_B(k)\int d^3r\, g(r)\eta(r)^2(\mathbf{l}\cdot\mathbf{r})(\mathbf{m}\cdot\mathbf{r})(e^{i\mathbf{l}\cdot\mathbf{r}}+e^{i\mathbf{m}\cdot\mathbf{r}}) \ , \tag{C7}$$

$$\sigma_{3ij}=\rho S_B(m)\int d^3r\, g(r)\eta(r)^2(\mathbf{k}\cdot\mathbf{r})(\mathbf{l}\cdot\mathbf{r})(e^{i\mathbf{m}\cdot\mathbf{r}}-e^{i\mathbf{l}\cdot\mathbf{r}})+\rho[S_B(m)-1]\int d^3r\, g(r)\eta(r)^2(\mathbf{k}\cdot\mathbf{r})(\mathbf{l}\cdot\mathbf{r})(1-e^{i\mathbf{k}\cdot\mathbf{r}}) \ , \tag{C8}$$

$$\sigma_{3in}=\rho S_B(l)\int d^3r\, g(r)\eta(r)^2(\mathbf{k}\cdot\mathbf{r})(\mathbf{m}\cdot\mathbf{r})(e^{i\mathbf{l}\cdot\mathbf{r}}-e^{i\mathbf{m}\cdot\mathbf{r}})+\rho[S_B(l)-1]\int d^3r\, g(r)\eta(r)^2(\mathbf{k}\cdot\mathbf{r})(\mathbf{m}\cdot\mathbf{r})(1-e^{i\mathbf{k}\cdot\mathbf{r}}) \ . \tag{C9}$$

[1] T. Greytak and J. Yan, Phys. Rev. Lett. **22**, 987 (1969).

[2] T. J. Greytak, R. Woerner, J. Yan, and R. Benjamin, Phys. Rev. Lett. **25**, 1547 (1970).

[3] C. A. Murray, R. L. Woerner, and T. J. Greytak, J. Phys. C **8**, L90 (1975).

[4] J. W. Halley, Bull. Am. Phys. Soc. **13**, 398 (1968); Phys. Rev. **181**, 338 (1969).

[5] F. Iwamoto, Prog. Theor. Phys. **44**, 1135 (1970).

[6] J. Ruvalds and A. Zawadowski, Phys. Rev. Lett. **25**, 333 (1970); A. Zawadowski, J. Ruvalds, and J. Solana, Phys. Rev. A **5**, 399 (1972).

[7] P. Kleban and R. Hastings, Phys. Rev. B **11**, 1878 (1975).

[8] J. W. Halley, in *Elementary Excitations in Quantum Fluids,* edited by K. Ohbayashi and M. Watabe, Springer-Verlag Series in Solid State Sciences Vol. 79 (Springer-Verlag, Berlin, 1989), p. 106.

[9] J. W. Halley and M. Korth, in *Excitations in Two-Dimensional and Three-Dimensional Quantum Fluids,* edited A. F. G. Wyatt and H. J. Lauter (Plenum, New York, 1990).

[10] M. Udagawa, H. Nakamura, M. Murakami, and K. Ohbayashi, Phys. Rev. B **34**, 1563 (1986).

[11] E. Manousakis and V. R. Pandharipande, Phys. Rev. B **30**, 5062 (1984).

[12] E. N. Manousakis and V. R. Pandharipande, Phys. Rev. **31**, 7029 (1985); **33**, 150 (1986).

[13] R. P. Feynman and M. Cohen, Phys. Rev. **102**, 1189 (1956).

[14] H. N. Robkoff and R. B. Hallock, Phys. Rev. B **24**, 159 (1981).

[15] P. Dacre, Mol. Phys. **45**, 17 (1982).

[16] M. J. Stephen, Phys. Rev. **187**, 279 (1969).

[17] W. H. Press *et al., Numerical Recipes* (Cambridge University Press, Cambridge, England, 1986).

[18] R. A. Cowley and A. D. B. Woods, Can. J. Phys. **49**, 177 (1971).

[19] K. Ohbayashi, M. Udagawa, and M. Watabe, Can. J. Phys. **65**, 1571 (1987).